RSC Advances

ROYAL SOCIETY OF CHEMISTRY

www.rsc.org/advances

RSC Advances

RSCPublishing

ARTICLE

Enhanced Vacuum Sensing Performance of Multiwalled Carbon Nanotubes: Role of Defects and Carboxyl Functionalization

Cite this: DOI: 10.1039/x0xx00000x

Received 25ht October 2014,
Accepted

DOI: 10.1039/x0xx00000x

www.rsc.org/

K.Rajavel[a],M. Dinesh[a], R. Saranya[a], and R.T. Rajendra kumar[a, b, c],

Defect controlled Multiwalled carbon nanotubes (MWCNTs) are synthesized by new modified one step pyrolysis method using ferrocene and xylene as effective precursors. Growth was performed in different pyrolysis temperatures (770-970°C). Morphological and structural characterization shows the formation of nanotubes with diameter and length about 10-80 nm and 0.2 to 2.0 µm respectively. MWCNTs grown at 870°C shows the higher graphitization degree (76%) with a lower defect density compared to other growth temperatures. Thermogravimetric and Fourier Transform Infrared Spectroscopy results reveal the formation of nanotubes with good structural quality and high quantity of carboxyl functional groups. The drop casted MWCNTs network based sensors are fabricated and studied for vacuum sensing properties. MWCNTs grown at 870°C show vacuum sensitivity of 26%. MWCNT vacuum sensor showed excellent reversibility with fast response and recovery time (20 sec) at room temperature. Our observation designates that arresting of carrier flow in MWCNTs by atmospheric O_2 adsorption at carboxyl functional sites and subsequent desorption of O_2 during vacuum which decreases the sensor resistance. Investigations explored that the presence of surface active carboxylic sites and nature of (ordered and defective) stacking of graphite layers in the nanotubes determines the vacuum sensing characteristics.

Introduction

Single layered and multiple layered structure of graphene sheet termed as carbon nanotubes (SWCNTs; MWCNTs) has been anticipated as a backbone for re-convolution of carbon based nanomaterial in carbon allotrope family. The extreme level of physical-chemical properties of CNTs such as high mechanical strength, low density, high specific surface area, excellent thermal and electrical conductivity has made them an excellent material for advanced devices.[1,2] CNTs have created a great impact on their potential applications such as field emission displays, sensory array, electronics, energy storage devices and biological applications.[3,4,5] For large scale utilization of CNTs, the ability to produce mass product with high structural quality at low cost with consistent reproducibility is required. So far, many approaches such as electric arc discharge, laser ablation, hot filament chemical vapour deposition (CVD) and plasma-enhanced CVD are used for controlling the production of SWCNTs, MWCNTs and doped CNTs.[6,7,8] Out of many fabrication approaches, pyrolysis is a modified method of CVD offers exotic advantages lined with large scale production, low cost, eco-friendly and also it requires moderate growth temperatures.[9,10,11,12,13]

Up to date, there is no experimental evidence in simple pyrolysis approach to control defect level in nanotube structures during the growth process itself. Defect controlled growth as well as production of CNTs in high pure quality is essential to expose their extraordinary properties. Besides, T. J. Yoon et al.,[14] C. P. Paul Wattset al.,[15] and P. G. Collins et al.,[16] observed change in nanotube network resistance upon varying the pressure while studying the gas sensing response of the CNTs. K. Takeshi et al.,[17] reported on MWCNT based electrothremal pressure sensor fabricated by local electric-field guided chemical vapour deposition, however the device fabrication involves multiple processing sequence viz. fabrication of suspended Si microstructure, doping the microstructure, catalyst deposition and local growth of MWCNTs on Si microstructures involve expensive lithographic processing techniques and complicated device fabrication methodology. In this present study, we report on vacuum sensor device fabricated by drop casting of simple, one step pyrolysis grown MWCNTs. We demonstrated that the vacuum sensitivity of the device can be enhanced by controlling the defects and surface functionalization of MWCNTs. MWCNT vacuum sensor shows fast response and recovery time with excellent reversibility at room temperature.

Results and Discussion

Structural Characterization of MWCNTs

Fig. 1(a and d, b and e, c and f) shows the TEM images of MWCNTs samples grown at 770, 870 and 970°C respectively. The diameter and length distribution of MWCNTs are calculated from TEM images using Image J software. The diameter and length of MWCNTs grown at 770°C are in the range of 10 to 60 nm and 0.2 to 1.6 µm respectively. And also the majority of nanotubes show poor structural quality with an inhomogeneous wall thickness (indicated in Arrow in Fig. 1(d)). On the other hand, the nanotubes grown at 870 and 970°C show well-ordered structure with uniform wall thickness and the diameter and length are in the range from 10-100 nm and 0.4 to 2 µm. (Fig. 1(b and c)). Increase in diameter and length distribution of nanotubes with increase in growth temperatures is clearly depicted from HRTEM images. These significant increases in tube diameter and length with increasing growth temperatures were also reported by J. L. Cheol et al.[18]

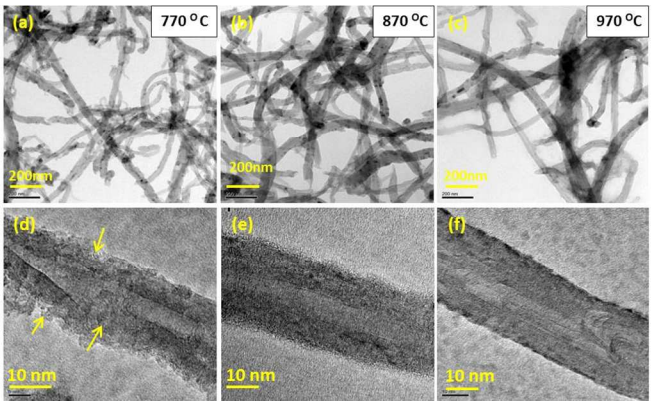

Fig. 1 Transmission Electron Microscopic images of MWCNTs grown at different growth temperatures (770 - 970°C).

X-ray Diffraction characterization

Fig. 2(a) shows the X-ray Diffraction (XRD) pattern of MWCNTs grown at different pyrolysis temperatures (770, 870 and 970°C). The peaks observed at 25, 42, 54 and 78° corresponds to (002), (101), (004) and (110) planes of CNTs respectively, which are well matched with JCPDS card no 75-1621 and 41-1487.[19] The d-spacing or interlayer spacing between two staked sp^2 graphene layers in MWCNTs is calculated using Bragg's law $n\lambda = 2dsin\,\theta$, where, d - distance between the planes of graphite layers, n- order of diffraction, λ - wavelength of X - ray light used, θ- Bragg angle and their calculated results are shown in Fig. 2(b). Nanotubes grown at 870°C shows lower 'd' spacing when compared with the other two growth temperatures (770 and 970°C). The calculated interlayer spacing of MWCNTs samples is lower when compared with pure graphite (3.3354 Å). Similar type of observation with the decrease of interlayer spacing for MWCNTs is reported by Zhi Wang et al.[19]

Graphitization degree is a method to quantify material changes from disordered graphite to a perfect graphite structure. The degree of graphitization is calculated from the Maire and Merings equation.[20] $g = \frac{0.3440 - d_{002}}{0.3440 - 0.3354}$ where, 0.3440 nm is the interlayer spacing of fully non-graphitized carbon, 0.3354 nm is an interlayer spacing of ideal graphite crystalline and d_{002} is an interlayer spacing derived from XRD (nm). The observed higher graphitization degree (76%) from the Fig. 2(b) for the sample grown at 870ºC on comparisons with other growth temperatures elucidates the well-ordered structure of MWCNTs.

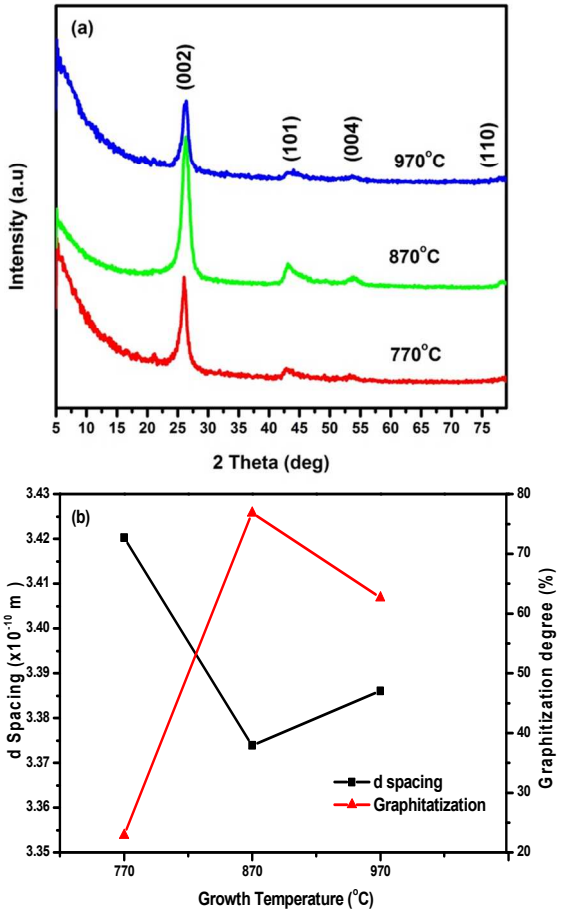

Fig. 2 (a) XRD pattern of pyrolysis synthesized MWCNTs at three different growth temperatures (770, 870 and 970°C) and corresponding peaks for respective plane is indexed. (b) Effect of temperature on interlayer 'd' spacing and graphitization degree of MWCNTs for (002) plane.

Raman Spectroscopy

Fig. 3(a) shows the Raman spectrum of MWCNTs grown at 770, 870 and 970°C. The peaks observed at 1350, 1580 and 2700 cm^{-1} are the characteristics peaks due to the scattering of defect (D band), tangential mode (G- band) and in plane terminations of disordered graphite (G|- band) of MWCNTs.[21,9] And also the second order vibrations band (G|) intensity is sensitive to the sample purity and/or defect density.[10] The intensity ratio between G and D peaks is used to evaluate the graphitization degree of carbon nanotubes.. The lower value of I_D/I_G consequently relates to the high quality of MWCNTs higher this value corresponds to poor structural quality,

which contain amorphous carbon and structural disorder.[9] MWCNTs grown at 870°C displayed a higher degree of the crystallinity compared to other samples grown at (770 and 970°C) expressed from the observed lower values of I_D/I_G (Fig. 3(b)). Further, the lower value of FWHM (Full Width at Half Maximum) and shift of Raman peak (G band) towards higher wave number associated with the sample grown at 870°C indicates good quality of MWCNTs.[22,23,24] The measured FWHM and shift in Raman peak position on effect of growth temperature is given in supportive information S1.

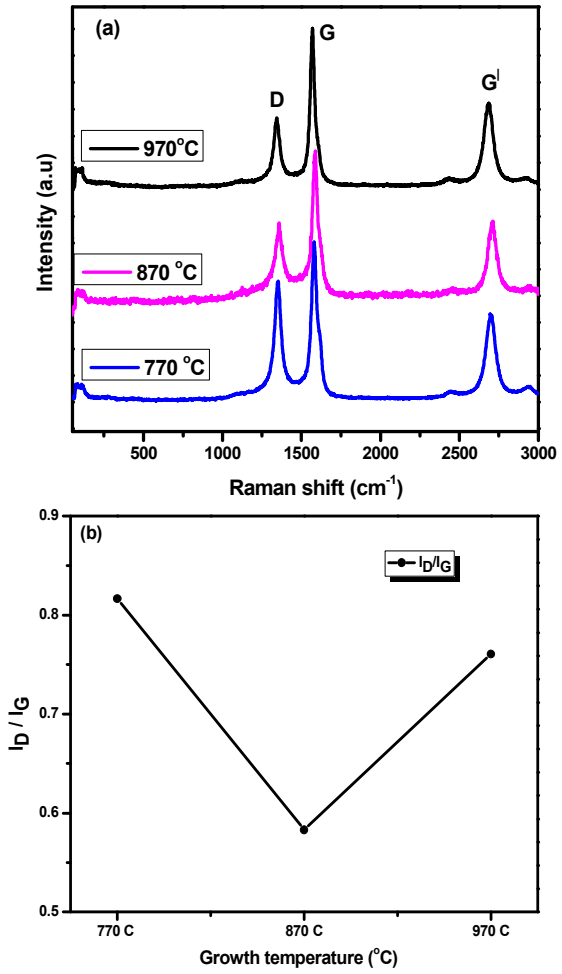

Fig. 3(a) Micro Raman spectra of pyrolysis synthesized, purified MWCNTs grown at 770, 870 and 970°C. (b) Influence on growth temperatures on I_D/I_G ratio of MWCNTs samples.

Thermogravimetric analysis

The evaluation of thermal stability as well as the material purity of CNTs is accessed from the thermogravimetric and differential thermal analysis (TGA/DTA). Fig. 4 (a) shows the TGA weight loss curve for MWCNTs grown at different pyrolysis temperatures (770, 870 and 970°C). MWCNTs grown at 770ºC show higher weight loss (~41% see supportive information S2) upon heated to 200°C compared with the samples grown at 870 and 970ºC. The observed rapid weight loss about 41% may be due to the evaporation of both amorphous carbon as well as the decarboxylation of carboxyl functional groups in nanotubes accompanied with the release of carbon dioxide.[25] Weight loss in the range upto ~18% was reported due to the decarboxylation from MWCNTs.[26] However, in our present study, the observed large variation in weight loss (41%) for MWCNTs grown at lower temperature (770°C) affirms the presence of carboxyl functional groups accommodated in defective nanotubes along with amorphous carbon. Whereas, minimum weight loss observed at 14% in the above said temperature range for 870°C grown MWCNTs samples confirms the presence of carboxyl groups. There is no weight loss observed for MWCNTs grown at 970°C attributed to absence of carboxyl groups.

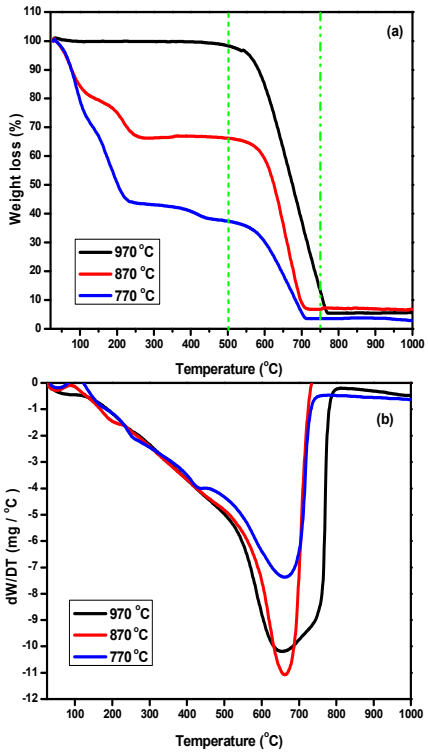

Fig. 4(a) The representative weight loss in TGA profile of MWCNTs grown at different growth temperatures (770, 870 and 970°C). (b) The differential weight loss curve obtained from the DTA profile for various growth temperatures (770, 870 and 970°C).

High quality CNTs possesses high oxidative stability (>550°C) which indicates the formation of nanotubes with well graphite structure.[27] Besides, the higher oxidative stability of nanotubes is clearly observed for samples grown in 870 and 970°C compared with lower growth temperatures (respectively for 770°C at 575°C; 870°C at 588°C and 970°C at 592°C) (Fig. 4(a)). It clearly renders that the samples grown at higher growth temperatures have a more acute oxidation rate and more stable due to their well graphitic structure. Similarly, the on-set temperature of the DTA spectra (Fig. 4(b)) of the samples grown at 770, 870 and 970°C found to be 517, 585 and 550°C respectively. The observed higher oxidation temperature of nanotubes grown at 870°C implies its relatively good structural quality compared with the samples grown at 770 and

970°C. It has been reported that higher oxidation temperatures belongs to high quality nanotube structures.[28] A notable broadening in the peak observed for the samples grown at 970°C may be due to the presence larger nanotubes diameter with more strain.[27,29] The calculated lower 'd' spacing (XRD analysis) and I_D/I_G ratio (Raman results) for the sample grown at 870°C further supports the formation of nanotubes structures with minimum defect density on compared with other growth temperatures. The assessed purity of grown MWCNTs in one step pyrolysis method is calculated from residual mass in TGA curve and it is found in the range of 94-96%.

Fourier Transform Infrared (FTIR) Spectroscopic Characterization

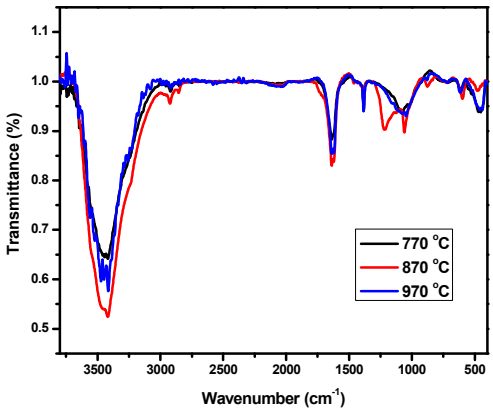

Fig. 5 FTIR transmittance spectra of MWCNTs grown at different pyrolysis temperatures (770-970°C) recorded in KBr pellet mode with a measured range from 400 to 4000 cm^{-1}.

Fig. 5 shows the FTIR transmittance spectra for the MWCNTs grown at 770, 870 and 970°C. The vibration band observed at 1637 cm^{-1} for all the samples corresponds to C=C vibrations mode, which originates from the backbone of CNTs.[29] Similarly, the band observed at 3417 cm^{-1} is attributed to the presence of O-H groups on the surface of nanotubes and it is believed to result from either ambient atmosphere, moisture bound to the nanotubes or by the vibration peak for the presence of water molecules.[29] The peak at 1381 cm^{-1} belong to O-H in plane bending of monomeric primary alcohol attachment on the nanotube surface. The vibration peak obtained at 1045 cm^{-1} for the samples grown at 970°C are identified as the side wall attachment O-H in single primary alcoholic groups or associated with ether R–O–R functionalities,[30] this feature is not observed for other growth temperatures. Whereas, the peaks observed at 1060 and 1077 cm^{-1} are assigned to the presence of carboxyl groups with vibrations of -COOH on MWCNTs for the growth temperatures (770 and 870°C) but this feature is not observed for higher growth temperature (970°C). The peak observed at 1215 cm^{-1} corresponds to the vibrations of carboxyl groups.[31] Interestingly, samples grown at 870°C show stronger band at 1215 cm^{-1} compared to the samples grown at 770 and 970°C corresponds to the presence of higher quantity of carboxyl functional groups.

Vacuum sensing

The vacuum response of the MWCNTs is studied by measuring the change in MWCNT resistance at room temperature by varying the pressure. Fig. 6(a) shows the vacuum response of MWCNTs grown at 770, 870 and 970°C measured in the pressure range 1000 to 0.04 mbar. The fabricated CNTs devices showed decrease in the measured resistance in a vacuum. Upon exposing to atmospheric pressure, the resistance of the nanotube device is reversed back to its initial value.

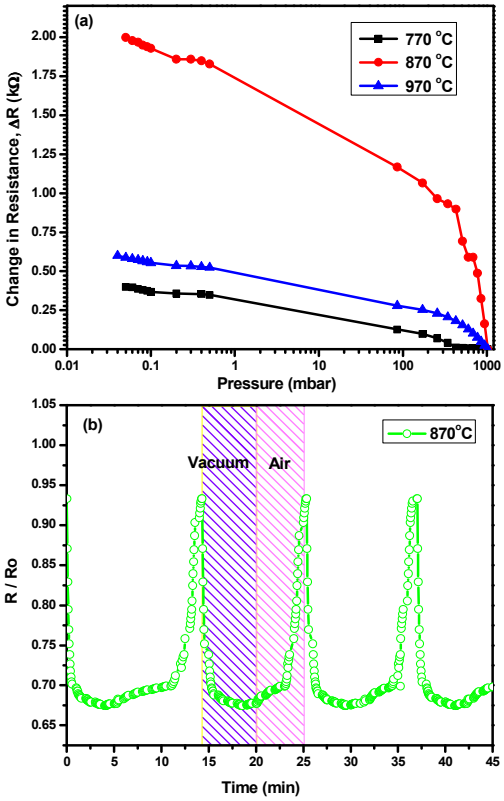

Fig. 6(a) The change in resistance for MWCNTs grown at 770, 870 and 970°C under pressure range from 1000 to 0.04 mbar for different growth temperatures. (b) Measured sensing response of fabricated MWCNTs grown at 870°C under vacuum and air exposure in repeated cycles of experiments.

The change in response observed for nanotube networks grown at 870°C is higher compared with other growth temperatures (770 and 970°C). The sensor devices fabricated based on MWCNTs grown at 770, 870 and 970°C show vacuum sensitivity of about 11, 26 and 13 % respectively. Dynamic response of nanotube network is analyzed by measuring the relative resistance change (R/R_o: R- is a change in resistance and R_o- is initial resistance) by varying pressure from 1000 to 0.04 mbar). Fig. 6(b) shows the dynamic response of the MWCNTs sample grown at 870°C. The reversible change in R/R_o values upon vacuum and venting process is observed for the fabricated CNTs devices. The resistance of the MWCNT based vacuum sensor changes continuously with pressure variation indicating a fast response and recovery time with good reversibility.

The vacuum sensing response of fabricated MWCNTs is compared with the commercial Pirani gauge response and shown in

Fig. 7. The MWCNT sensor show sharp decrease in measured R/R_o values on decreasing the pressure from 1000 to 0.5 mbar and saturates on further decreasing the pressure. The results indicate that the MWCNT vacuum sensor show good response in the pressure window range from 1000 to 0.5 mbars. MWCNT sensor show fast response and recovery time about 20 sec. The present results are compared with previous reports and tabulated in table 1.

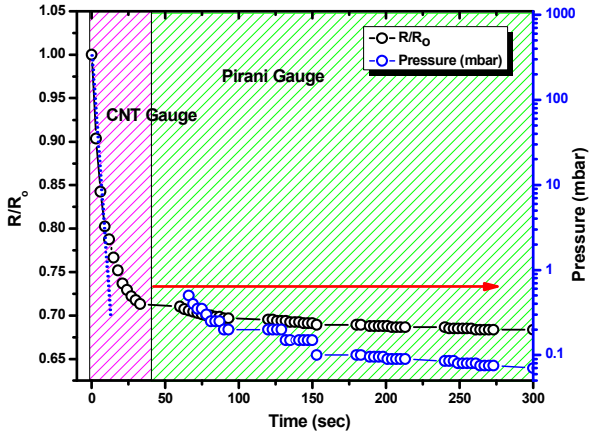

Fig. 7 Vacuum sensing response of MWCNT networks as function of pumping time and their active window for pressure detection limit correlation with standard Pirani gauge.

Discussion

Pyrolysis growth of CNTs is explained in gas phase surface reaction by the process of dissolving; diffusion and precipitation of carbon atoms in the presence of catalytic iron particles.[36] At a lower growth temperature (770°C), thermal decomposition of hydrocarbon are slow which is attributed to the minimum probability of carbon and catalyst particle interaction which hampers the nanotube growth. As the decomposition is slow, the supply of carbon atoms to the Fe catalysts is less resulting in the growth of defects MWCNTs (Fig. 1(d)) with non-uniform diameter along with the formation of other carbon nanoparticles and impurities such as amorphous carbon and graphite particles.[33] On increasing the growth temperature to 870°C, the supply of carbon atoms is increased and attain equilibrium of dissolving and diffusion rate to catalyst thus favors the formation of the well graphitic nature of nanotubes with minimum defect density (Fig. 3(b)) supported from TEM results (Fig. 1(e)). On further increasing the growth temperature to 970°C, the higher dissolving rate of hydrocarbon compared with diffusion and precipitation rates leads to the increase of CNT growth rate along with the deposition of more amorphous carbon.[7,10,17,36] This can be verified from the large weight loss of the sample grown at 970°C compared to the samples grown at 870°C during the dry oxidation process (see supportive information S3). The aforementioned growth mechanism established the fact of formation of higher quality nanotubes at moderate growth temperature (870°C).

The vacuum sensing properties of defect controlled nanotubes influenced by different growth temperatures are analyzed. The samples grown at moderate growth temperatures (870°C) showed higher vacuum sensing response compared to samples grown at other temperatures (770 and 970°C). The remarked higher vacuum sensing response of our fabricated CNTs device (870°C) is demonstrated by the available number of carboxyl surface active polar sites. The results from TG/DTA and FTIR (Fig. 4 and 5) clearly indicate the effective carboxyl functionalization on nanotube surfaces during purification. As such, the availability of a number of carboxyl groups present in the nanotubes can readily adsorb atmospheric O_2 molecules which arrest carrier flow in nanotubes explored by a measured increase in CNTs sensor resistance. In general, the adsorption of oxygen molecules on nanotube surface is explained on p - semiconducting nature of oxygen doping effect.[16] During the vacuum process, desorption of physisorbed O_2 from the functional sites (i.e.) in the carboxyl functionalized CNTs enhance the hole carrier concentration which release the conduction block leads to decrease in CNTs network resistance. On the other hand, the samples grown at 770°C also possess carboxyl functional groups, verified from the analysis of FTIR and TG/DTA during the purification process, but it suffers with irregular nanotube structure with a high defect density (Fig. 1(a) and (d)), and therefore shows lower vacuum sensitivity. The samples grown at higher growth temperatures (970°C) show relatively lower vacuum sensitivity compared to CNTs grown at 870°C. This could be due to the minimum surface functional groups present in the nanotube structures. Thus, the well-ordered good quality nanotube structures with a minimum quantity of carboxyl functional active sites in nanotubes are not much involved in physisorption with atmospheric O_2. In essence, vacuum sensitivity of CNTs depends on (1) number of carboxyl sites at nanotube surface and (2) lattice defects which influence the oxygen interaction and carrier transport respectively. The CNTs grown at 870°C possess an excellent combination of carboxyl sites at the surface with a good structural quality exhibit in enhanced vacuum sensitivity. Whereas the CNTs grown at 770°C suffers with poor structural quality and samples grown at the 970°C lack of surface carboxyl active sites display relatively poor vacuum sensitivity.

Materials and Methods

Growth of Carbon nanotubes

Ferrocene and xylene are purchased from Sigma Aldrich and SD fine, India; are used as received. The schematic of one step modified pyrolysis apparatus along with the quartz tube reactor (800 mm (L) x 450 mm (ID)) is used in the present study as shown in Fig. 8. A movable thermocouple is used to establish the temperature profile of the furnace (Fig. 8) and its effective operating region in middle of quartz tube is about 100 mm. The mixtures of ferrocene (3 weight%) and xylene are used as a starting material and placed in front of the quartz tube reactor. Before starting reaction, the quartz tube is flushed with Ar (2.5 ml/min) about 10 minutes in order to create oxygen free environment. The vaporized carbon and catalyst mixtures are carried to high temperature zone with carrier inert gas. Synthesis of CNTs carried out in different pyrolysis temperatures ranges 700-1000°C in atmospheric pressure. After 1h reaction time,

heating is turned off and the reactor is warmed down gradually to room temperature under Ar flow. Thick and uniform black surfaces of MWCNTs formed on the inner wall of the quartz tube in the central core region of the furnace. The collected carbonaceous materials are quantified and subjected to the purification process.

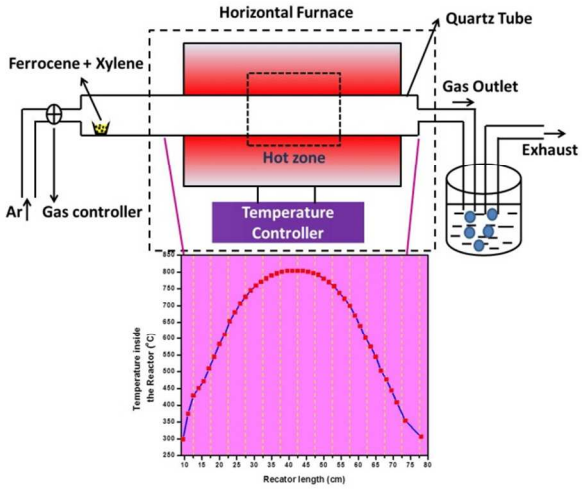

Fig. 8 Illustrations of modified pyrolysis apparatus used for synthesis of MWCNTs and their temperature profile.

The raw product contains aerogel support, catalyst particles and small amount of amorphous carbon impurities. In order to remove those impurities, the samples are purified by heating in air atmosphere at 450ºC for 2h to remove the amorphous carbon and their respective weight loss in different dry oxidation process is quantified. In order to remove the catalyst metal particles, acid assisted purification process performed in mixtures of HNO_3 and H_2SO_4 (1:3) is reported.[37,38] The acid refluxed CNT suspensions are filtered and washed several times with copious amount of distilled water until the pH of the filtrate to neutral. Finally filtrate membranes are dried in oven at 60°C for 12h. These dried samples are further subjected to XRD, TEM, FTIR, Raman and TGA/DTA characterization. Details of the characterization procedures are included in Supportive information S4.

Sensor Fabrication and Testing

Purified MWCNTs are dispersed in N, N-dimethylformamide solution with the concentration ratio of 0.1 mg/ml. This suspended solution is applied to bath sonication (Rivotech India Ltd.) about 4h for better dispersion. Uniformly dispersed solutions are drop casted on the prefabricated silver electrode (170 nm thick) assembly with inter electrode spacing about 350 µm. The vacuum sensing properties of CNTs electrode assembly are done by using simple, homemade setup with the help of rotary pump connected (200L/min (50 Hz)) to a thermal evaporation vacuum chamber (35 x 31cm). The variation in resistance to the corresponding vacuum pressure for each sample are measured using Agilent data acquisition (Model: 34970A) unit family. The sensitivity of our CNTs electrode assembly is calculated at 1 mbar according to formula (1). Where, R_{air} – resistance in air, R_{vacuum} – resistance in vacuum.

$$Sensitivity = \frac{R_{air} - R_{vacuum}}{R_{air}} \times 100\% ----(1)$$

Conclusion

One step, simple method is adopted for the defect controlled, bulk production of MWCNTs. The influence of pyrolysis temperature on the alignment, structural quality, defects and surface active sites of synthesized MWCNTs are analysed. Vacuum sensing properties of MWCNT based devices reveal that the available surface active sites and structural quality are responsible candidates for their enhanced vacuum sensing performance. MWCNT vacuum sensor show sensitivity of 26% with response and recovery time of about 20 sec. These results indicate that on further analysing the electrode-CNT interface, CNT percolation pathways and intertube contacts with improved device architecture can result in a new class of vacuum monitoring devices..

Acknowledgement

One of the authors, K. Rajavel acknowledges Council for Science and Industrial Research (CSIR), New Delhi, for the award of Senior Research Fellowship.

References

1. P. A. Loiseau, P. P. Launois, J. P. S Roche, (Eds.). *Understanding Carbon Nanotubes,* Springer: Netherland, Verlag, Berlin Heidelberg press, 2006.
2. Peter J and Harris F. Carbon Nanotube Science Synthesis, Properties and Applications; Cambridge University Press, 2009.
3. M. A. Pulickel, and Z. Z. T. Otto, *Appl. Phys.,* 2000, **80**, 391–425.
4. K. Rajavel, R. Gomathi, S. Manian, and R. T. Rajendrakumar, *Langmuir,* 2014, **30**, 592-601.
5. K. Rajavel, C. R. Minitha, K. S. Ranjith, and R. T. Rajendra Kumar, *Recent Patents on Nanotechnology,* 2012, **6**, 99-104.
6. N. M. Mubarak, Y. Faridah, and Y. E. Alkhatib, *Chemical Engineering Journal,* 2011, **168**, 461-469.
7. H. Haoqing, K. Andreas Schaper, W. Frank and G. Adreas, *Chem. Mater.,*2002, **14**, 3990-3994.
8. A. Barreiro, D. Selbmann, T. Pichler, K. Biedermann, T. Gemming, M. H. Rummeli, et al. *Applied Physics A,* 2006, **82**, 719-725.
9. Z. D. Hu, Y. F. Hu, Q. Chen, X. F. Duan, and L. M. Peng, *J. Phys. Chem. B,* 2005, **110**, 8263-8267.
10. C. Castro, M. Pinault, S. Coste-Leconte, D.Porterat, N. Bendiab, C. Reynaud, and C. Mayne-L'Hermite, *Carbon,* 2010, **48**, 3807–3816.
11. S. Chaisitsak, J. Nukeaw, and A. Tuantranont, *Diamond and Related Materials,* 2007, **16**, 1958-1966.
12. K. Kazunori, E. Hajime, S. Kozo, Q. Dali, A. Rodney, and A. EricGrulke, *Carbon,* 2005, **43**, 253–260.
13. A. Zahab, L. Spina, P. Poncharal, and C. Marliere, C, *Physical Review B,* 2000, **62**, 15.

14. T. J. Yoon, I. M. Seung, H. A. Jin, L. H. Yun, and K. J. Byeong, *Sensors and Actuators B,* 2004, **9**, 118–122.
15. C. P. Paul Watts, M. Natacha, T. Zhenni, M. Yoji, J. C. David, and P. S. Ravi, *Nanotechnology,* 2007, **18**, 175701.
16. P. G. Collins, K. Bradley, M. Ishigami, and A. Zettl, *Science,* 2000, **287**, 1801-4.
17. K. Takeshi, C. Hether, Q. Z. Marcel, D. S. Brain, Sosnowchik and Liwei, Lin, *Nano letters,* 2007, 7**,** 3686-3690
18. J. L. Cheol, P. Jeunghee, H. Yoon, and Y. L. Jeong, *Chemical Physical Letters,* 2001, **343**, 33-38.
19. W. Zhi, Wang. B. Dechun, L. Fei, C. Peijiang, Y. Tianzhong, G. Yousong, and et al., *Vacuum,* 2005, 77, 139–144.
20. F. Y. Wu, and H. M. Cheng, *J. Phys. D: Appl. Phys.,* 2005, **38**, 302–4307.
21. H. L. John, M. K. Elisabeth, E. Hurst, and M. Vincent, *Carbon,* 2011, **49**, 2581–2602.
22. C. Singh, M. S. P. Shaffer, and A. H. Windle, *Carbon,* 2003, **412**, 359–68.
23. J. Judek, C. Jastrzebski, A. Malolepszy, M. Mazurkiewicz, L. Stobinski, M. Zdrojek, Phys. Status Solidi A, 2012, **209**, 313–316.
24. O. Sebastian, H. Mickael, and G. Yury, *J. Raman Spectrosc.,* 2007, **38**, 728–736.
25. S. K. LouisPang, D. John Saxby, and C. S. Peter, *The Journal of Physical Chemistry,* 1993, **97,** 27.
26. Y. Rike, O. Holia, Y. Sudirman, S. Yukie, I. Tadahisa, and A. Jun-ichi, *The Open Materials Science Journal,* 2011, **5**, 242-247.
27. K. DilipSingh, K. I. Parameswar, and P. K. Giri, *Journal of Applied Physics,* 2010, **108**, 084313.
28. S. A. Duha, J. H. Adawiya, and M. R. Mohammad, *Energy Procedia.,* 2013, **36**, 1111–1118.
29. R. G. R. Goyanes, A. J. Salazar, M. A. Corcuera, and I. Mondragon, *Diamond and Related Materials,* 2007, **16**, 412–417.
30. A. A. Faraj, L. Tahar,A. H. Mamdouh, and A. A. Muataz, *The Arabian Journal for Science and Engineering,* 2010, **35**, 37-48.
31. B. T. Nuruzatulifah, M. Asari T. Jean-Philippe, R. Ali, R. R. Sylvia, and M. G. Kutty, *Sains Malaysiana,* 2012*,* **41**, 603–609.
32. C. Jungwook and K. Jongbaeg, *Nanotechnology*, 2010, **21**, 105502.
33. B. K. Anupama, *IEEE Transactions on Nanotechnology*, 2009, **8,** 252-257.
34. S. J. Chang, T. J. Hsueh, C. L. Hsu, Y. R. Lin, I. C. Chen, and B. R. Huang, *Nanotechnology,* 2008,**19,** 095505.
35. M. A. Ponce, R. Parra, R. Savu, E. Joanni, P. R. Bueno, M. Cilense, J. A. Varela, M. S. Castroa,*Sensors and Actuators B*, 2009, **139**,447–452.
36. I. I. Mihnea, Z. Yong, L. Ruying, S. Xueliang, A. Hakima, and S. L. Lussier, *Applied Surface Science,* 2011, **257**, 6843–6849.
37. V. Datsyuk, M. Kalyva, K. Papagelis, J. Parthenios, D. Tasis, A. Siokou, A, and et al., *Carbon,* 2008, **46**, 833–840.
38. L. Yu, Z. Xiaobin, L. Junhang, H. Wanzhen, C. Jipeng, L. Zhiqiang, and et al., *Nanotechnology,* 2004, **15**, 1645–1649.

Table 1. Sensor parameters Comparison with reported pressure sensors.

Sensor Materials	Measurement Range (mbar)	Sensing response	Response /Recovery time	Operating Temp.	Farbication and Working principle
MWCNTs[32]	2.5x 10^{-5} to 100	~2 %	10/20 Sec	-----	Micro fabricated, electrothermal thermistor
MWCNTs[17]	0.0001 to 100	~13%	----/----	-----	CMOS based Electrothermal thermistor
SWCNTs[33]	0. 000001-1013	1 nA per 1.33 mbar	----/----	<27°C	Microfabricated FET
ZnO Nanowire[34]	0.01 to 1333	23%	----/----	27°C	Lithography assisted fabrication, Resistive pressure sensor
TiO_2[35]	0.133 to 1000	3 orders of response	----/----	350ºC	Thin films based sensor, Change in impedance
SWCNTs[16]	1.3 x 10^{-6} -1000	~10 to 15%	----/----	76°C	Random Networked Resistive sensor
MWCNTs (Present Study)	0.04 to 1000	26%	20/22 Sec	27ºC	Random Networked Resistive sensor